Available online at www.sciencedirect.com
ScienceDirect
Trans. Nonferrous Met. Soc. China 33(2023) 1492−1506
Transactions of Nonferrous Metals Society of China
www.tnmsc.cn

Phase equilibria of Zr−Co−Ge ternary system at 1023, 1173 and 1373 K

Kun HU[1], Chen SHEN[2], Hua-shan LIU[1], Hong-bin ZHANG[2]

1. School of Materials Science and Engineering, Central South University, Changsha 410083, China;
2. Institute of Materials Science, Technical University of Darmstadt, 64287 Darmstadt, Germany

Received 14 November 2021; accepted 1 March 2022

Abstract: Phase equilibria of the Zr−Co−Ge ternary system at 1023, 1173 and 1373 K were precisely measured via alloy sampling associated with electron probe microanalysis (EPMA) and X-ray diffraction (XRD) techniques. The isothermal sections in the Zr−Co−Ge system were appropriately constructed, containing 29, 28, and 26 three-phase regions at 1023, 1173, and 1373 K, respectively. Except for confirming the five ternary compounds previously reported in the literature, a new ternary phase τ was detected with a remarkable homogeneity range, consisting of 13.8−19.4 at.% Co at 1023 K, 12.9−19.0 at.% Co at 1173 K and 12.3−14.9 at.% Co at 1373 K. And, an invariant reaction was deduced to occur at a temperature between 1023 and 1173 K, i.e., $\tau+\tau1\rightleftharpoons\tau4+ZrGe_2$. Besides, the third element Ge can partly substitute Co in some Co−Zr intermediate phases, e.g., $CoZr_2$ and $Co_{23}Zr_6$ where the maximum solubility of Ge can separately reach up to 22.8 at.% and 20.3 at.%, respectively.

Key words: Zr−Co−Ge ternary system; phase diagram; compound; solubility

1 Introduction

Cobalt−zirconium-based (Co−Zr based) rare earth (RE) free alloys are of great scientific and applied values to serve as a permanent magnet material owing to their high Curie temperature and coercivity, remarkable oxidation and corrosion resistance, and large magneto-crystalline anisotropy energy (MAE) [1−4]. However, how to balance the coexistence of high coercivity and high magnetic energy product, explore the origin and mechanism of high coercivity in such alloys, and study the stability of magnetic phases are still rarely known and urgently needed to be solved, which hinder the development of practical applications more difficulty [5−7]. Therefore, a class of suitable alloying elements and optimized preparation techniques need to be utilized to enhance the comprehensive performance of such magnetic materials [8−10]. For example, by employing the alloying RE-free element Ge, not only the stability of magnetic phases is improved, e.g., $Co_{23}Zr_6$ and $Co_{11}Zr_2$, but several new ternary compounds are as well-formed potentially, e.g., Zr_2CoGe, $Zr_4Co_4Ge_7$, in the Zr−Co−Ge ternary system. In the meantime, a product with high coercivity and magnetic energy applications can be obtained [11−31]. Nevertheless, the stability of temperature and composition regions of the intermediate phases and their related phase equilibria in the Zr−Co−Ge ternary system were hardly reported. Even so, phase relations in the Zr−Co−Ge system are necessary to be accurately acquired. The influence of alloying element Ge can thus be further studied, which shows the potential to assist the application of Co−Zr-based RE-free permanent magnet materials in the future. In this work, a measurement of phase equilibria in the Zr−Co−Ge ternary system is implemented.

Heretofore, the relative binary phase diagrams of the Zr−Co−Ge system have been widely studied through experimental determination and crucial

Corresponding author: Hua-shan LIU, Tel: +86-731-88876735, Fax: +86-731-88876692, E-mail: hsliu@csu.edu.cn
DOI: 10.1016/S1003-6326(23)66198-9

thermodynamic assessments in Table 1. Besides the terminal solution phases (α-Zr), (β-Zr), (α-Co), and (ε-Co), there are six intermetallic compounds, $CoZr_3$, $CoZr_2$, CoZr, Co_2Zr, $Co_{23}Zr_6$ and $Co_{11}Zr_2$, regardless of the metastable Co_5Zr, in the Co−Zr binary system [13−15]. As for the Zr−Ge binary system, phase equilibria and crystal structure data of intermediate phases have been strictly identified and accepted, which contains five intermetallic compounds, Zr_3Ge, Zr_5Ge_3, Zr_5Ge_4, ZrGe and $ZrGe_2$, and the terminal solution phases (α-Zr), (β-Zr) and (Ge) [16−19]. Recently, the stability of intermediate phases and solid solution phases in the Co−Ge system was experimentally and theoretically investigated, covering Co_3Ge, Co_2Ge, Co_5Ge_2, Co_5Ge_3, CoGe, Co_5Ge_7 and $CoGe_2$, together with

Table 1 Crystallographic data of solid solution phases, intermetallic phases, and pure elements in Zr−Co−Ge ternary system

Phase	Pearson symbol	Space group	Prototype	Lattice parameter/nm			Comment	Ref.
				a	*b*	*c*		
(β-Zr)	cI2	$Im\bar{3}m$	W	0.3120	0.3120	0.3120		[18]
(α-Zr)	hP2	$P6_3/mmc$	Mg	0.3234	0.3234	0.5153		[19]
(α-Co)	cF4	Fm_3m	Cu	0.3544	0.3544	0.3544		[32]
(ε-Co)	hP2	$P6_3/mmc$	Mg	0.2506	0.2506	0.4080		[32]
(Ge)	cF8	$Fd\bar{3}m$	C	0.5651	0.5651	0.5651		[33]
$CoZr_3$	oS16	$Cmcm$	Re_3B	0.3270	1.0840	0.8950		[34]
$CoZr_2$	Zr12	$I4/mcm$	Al_2Cu	0.6363	0.6363	0.5469		[35]
CoZr	cP2	$Pm\bar{3}m$	CsCl	0.3163	0.3163	0.3163		[34]
Co_2Zr	cF24	$Fd\bar{3}m$	$MgCu_2$	0.6923	0.6923	0.6923		[36]
$Co_{23}Zr_6$	cF116	$Fm\bar{3}m$	$Mn_{23}Th_6$	11.480	11.480	11.480		[34]
$Co_{11}Zr_2$	oP	$Pcna$	Zr_2Co_{11}	0.4710	1.6700	2.4200		[37]
Zr_3Ge	tP32	$P4_2/n$	Zr_3P	1.1080	1.1080	0.5480		[16]
Zr_5Ge_3	hP16	$P6_3/mcm$	Mn_5Si_3	0.7993	0.7993	0.5594		[16]
Zr_5Ge_4	tP36	$P4_12_12$	Zr_5Si_4	0.7238	0.7238	1.3154		[16]
ZrGe	oP8	$Pnma$	FeB	0.7068	0.3904	0.5396	β=101.1°	[16]
$ZrGe_2$	oS12	$Cmcm$	$ZrSi_2$	0.3789	1.4975	0.3761		[16]
Co_3Ge	cF4	$Pm\bar{3}m$	Co_3Zr	−	−	−		[20]
$CoGe_2$	oC24	$Aba2$	$PdSn_2$	0.5670	0.5670	1.0796		[33]
Co_5Ge_7	Zr24	$I4mm$	Co_5Ge_7	0.7641	0.7641	0.5814		[33]
CoGe	mS16	$C2/m1$	CoGe	1.1650	0.3807	0.4945		[23]
β-Co_5Ge_3	hP6	$P63/mmc$	Ni_2In	−	−	−		[33]
Co_2Ge	oP12	$Pnma$	Co_2Si	0.5020	0.3820	7.2600		[22]
$Zr_4Co_4Ge_7$ (τ1)	Zr60	$I4/mmm$	$Zr_4Co_4Ge_7$	13.2280	13.2280	5.2290		[24]
$Zr_6Co_{16}Ge_7$ (τ2)	cF116	$Fm\bar{3}m$	$Mn_{23}Th_6$	11.6200	11.6200	11.6200		[25]
$ZrCo_6Ge_6$ (τ3)	hP13	P_6/mmm	Fe_6Ge_6Mg	5.0610	5.0610	7.8080		[26]
ZrCoGe (τ4)	oP12	$Pnma$	MgSrSi	6.5260	3.9300	7.2780		[27]
$Zr_4Co_7Ge_6$ (τ5)	cI34	$Im\bar{3}m$	$Re_7U_4Si_6$	7.8860	7.8860	7.8860		[28]
Zr_2CoGe	cF16	$F4\bar{3}m$	Li_2AgSb	6.7880	6.7880	6.7880		[30]
τ	−	−	−	−	−	−		This work

β is the angle between lattice parameters *a* and *c*

(α-Co), (ε-Co) and (Ge) [20−23]. In consideration of the phase relations and boundary of these constituting related binary systems that have been adequately accepted, phase diagrams of the related Co−Zr [13], Zr−Ge [16] and Co−Ge [20] binary systems are presented in Fig. 1 [20].

However, phase equilibria of the Zr−Co−Ge ternary system have barely been reported. Thus far, only five existed ternary compounds, i.e., $Zr_4Co_4Ge_7$ [24], $Zr_6Co_{16}Ge_7$ [25], $ZrCo_6Ge_6$ [26], ZrCoGe [27], $Zr_4Co_7Ge_6$ [28], and one predicted Heusler Zr_2CoGe phase [29−31], with their crystal structure, have been experimentally and theoretically confirmed, respectively. But referring to the stability along with the temperature changes and composition regions of such ternary compounds, the corresponding phase equilibria in the Zr−Co−Ge ternary system were barely studied.

As was previously discussed, our present work was mainly focused on systematic measurement of the phase equilibria in the Zr−Co−Ge ternary system at 1023, 1173, and 1373 K with the help of alloy sampling. The present work can be interesting and adopted to not only the professional researchers who focused on the investigation of phase diagram field but also experts who concerned in developing specialized composition design of alloys and related technically valuable in the thermodynamic study.

2 Experimental

Fine metal particles with high purity (Zr: 99.99%; Co: 99.99%; Ge: 99.999%, China New Metal Materials Technology Co., Ltd.) were employed to prepare a series of alloy buttons with different compositions, each with a mass of 8 g. The pre-determined amount of the alloy sample was placed in a vacuum chamber utilizing arc melting on a water-cooled copper plate. To ensure preferable homogeneity and a much less mass deviation (not exceeding 1%) in the alloys, those samples were turned over at least three times before each melting and remelted under the protection of titanium sponge and argon atmosphere. Straight after that, no less than 30 cut as-cast samples were uniformly sealed in evacuated quartz capsules and followed by

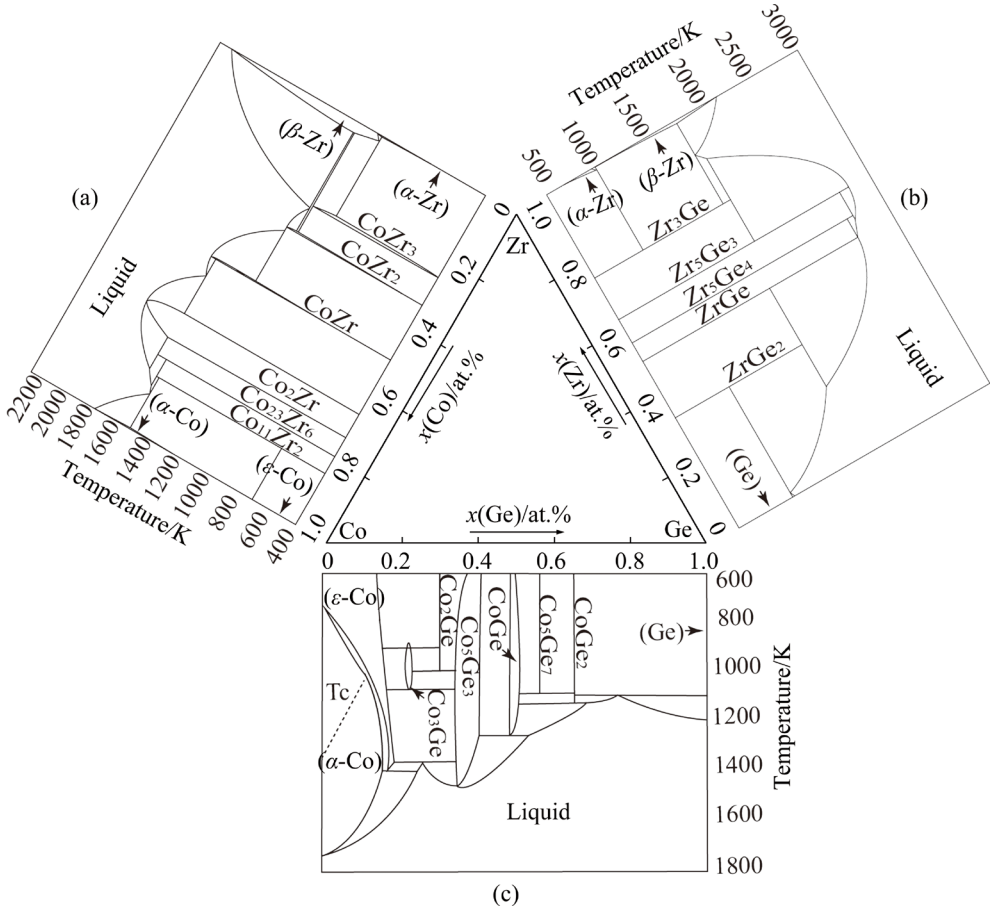

Fig. 1 Binary phase diagrams of Zr−Co−Ge ternary system: Zr−Co (a) [13], Zr−Ge (b) [16] and Co−Ge (c) [20]

heat-treatment at 1023, 1173, and 1373 K (with the error of ±3 K) for 90, 60, and 10 d, respectively. The annealed alloys in quartz tubes were taken out of the furnace and immediately broken and quenched in ice water to assure the phase equilibria at high temperature to be preserved entirely.

The constituent phases of the equilibrated alloys and their compositions were evaluated by electron probe microanalysis (EPMA) (JXA−8800R, JEOL, Japan) with OXFORD INCA 500 wavelength dispersive X-ray spectrometer (WDS). To guarantee the accuracy and reliability of experimental data, the total molar fraction of Zr, Co, and Ge in each phase is in the range of 97%−103% with the standard deviations of the verified concentration ±0.6 at.%. In the meanwhile, X-ray diffraction (XRD) was implemented to discern the phase character and differentiate the co-existing phases, using Cu K_α radiation on an X-ray diffractometer (Rigaku D-max/2550 VB+) in the continuous mode with a step size of 0.02° at a speed of 8 (°)/min, 40 kV, and 250 mA.

3 Results and discussion

After the adequate annealing duration, more than 30 typical equilibrated alloys covering almost the whole composition area have been adopted to estimate the phase equilibria of the Zr−Co−Ge ternary system at 1023, 1173, and 1373 K. What's more, the alloys which repeated the already existing two-phase or three-phase regions would not be presented in this manuscript. Strictly speaking, each alloy sample only occurs in one three-phase or two-phase microstructure, indicating the approaching or nearby approaching full equilibrium, except for alloys comprising the liquid phase. Moreover, in this work, five ternary compounds, i.e., $Zr_4Co_4Ge_7$ (τ1), $Zr_6Co_{16}Ge_7$ (τ2), $ZrCo_6Ge_6$ (τ3), ZrCoGe (τ4) and $Zr_4Co_7Ge_6$ (τ5), have been further ascertained with a specific range of compositions.

3.1 Phase equilibria at 1023 K

Phase equilibria of the constituent phases in the Zr−Co−Ge ternary alloys annealed at 1023 K for 90 d were analyzed. The microstructure of Alloy A2 with a nominal composition of $Zr_{62}Co_{14}Ge_{24}$ was outlined in Fig. 2(a). As the backscattered electron image (BSE) illustrated, three phases, including the white Zr_5Ge_3, gray $CoZr_2$, and black CoZr coexist. It is thus deduced that Alloy A2 should locate in the three-phase region of Zr_5Ge_3+$CoZr_2$+CoZr, in accordance with its XRD pattern as displayed in Fig. 2(b). Likewise, Fig. 2(c) presents

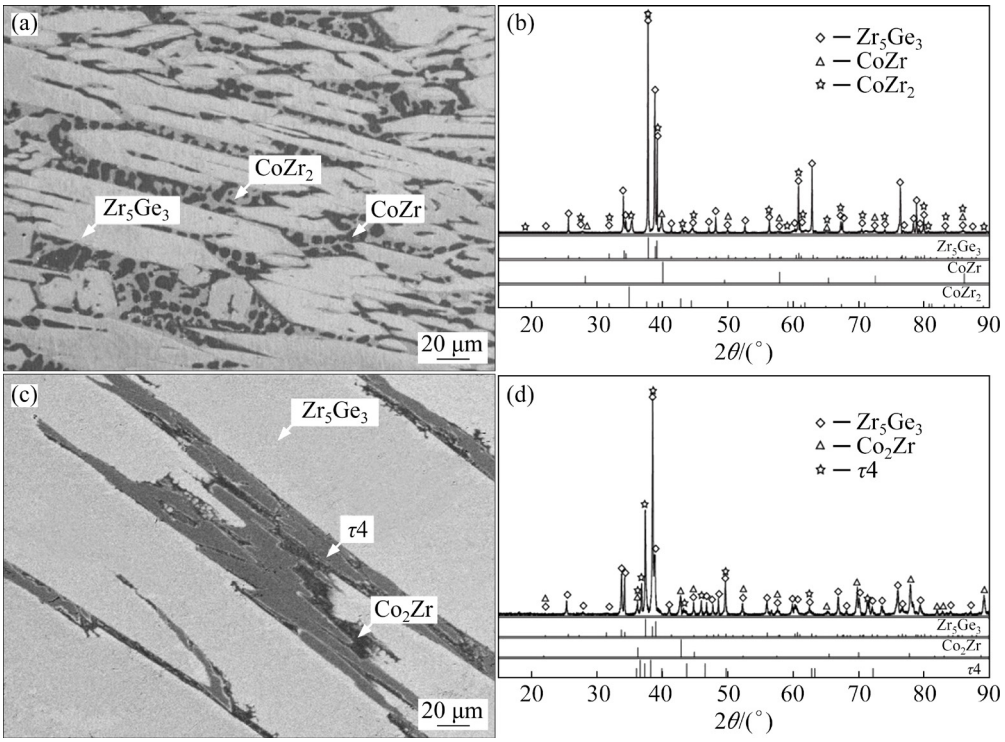

Fig. 2 BSE images (a, c) and XRD patterns (b, d) of typical alloys annealed at 1023 K for 90 d: (a, b) Alloy A2; (c, d) Alloy A6

a BSE image of Alloy A6, which encompasses white Zr_5Ge_3, black Co_2Zr, and the dark gray τ4 phase with the composition of 33.5Zr−35.6Co−30.9Ge (at.%). Combining with the XRD analyses (see Fig. 2(d)), it is apparent that alloy A6 locates in the three-phase area of Zr_5Ge_3+Co_2Zr+τ4.

Figures 3(a) and (b) revealed the coexisting phases in Alloy A16 of the nominal composition of $Zr_9Co_{15}Ge_{76}$. The dark gray $CoGe_2$ and matrix gray (Ge) phases could be distinguished, and a significant rod-like white τ1 phase was observed, hinting at a three-phase equilibrium $CoGe_2$+(Ge)+τ1. Although some tiny dispersive holes in this alloy due to Ge content led to brittleness, they exert little effect on the measurement of the composition of the equilibrated phases.

Figure 3(c) presents the microstructure of Alloy A20, which contains black gray τ1, gray $ZrGe_2$, and an unknown white phase with the composition of 44.1Zr−13.8Co−42.1Ge (at.%). The presence of holes does not affect the analysis of the composition of constituent phases. After excluding the diffraction peaks of the detected τ1 and $ZrGe_2$ phases, some characteristic peaks remain unidentified, which should belong to the unknown phase. So, the unidentified phase in A20 was considered a ternary phase and named τ phase hereafter. The τ phase was also detected in Alloys A7, A8, and A19.

Detected phases and their matching compositions in various annealed alloys at 1023 K are manifested in Table 2. Associating the phase equilibria obtained through alloy sampling with the relevant binary systems in literature, the isothermal section of the Zr−Co−Ge ternary system at 1023 K was established as characterized in Fig. 4, which consists of 29 three-phase regions. Specifically, the composition range of 6 ternary phases has been determined, of which the composition range of the new ternary phase τ has been roughly deduced, accompanied by 41.0−44.1 at.% Zr, 13.8−19.4 at.% Co and 39.6−42.1 at.% Ge at 1023 K. Besides, magnetic phase $Co_{23}Zr_6$ is stable with the third element Ge solubility about 12.0 at.%. It should be admitted that, although the three-phase regions, e.g., Zr_3Ge+$CoZr_2$+Zr_5Ge_3, τ+Zr_5Ge_4+ZrGe, τ+τ1+τ4, CoGe+τ3+$CoGe_2$, τ2+τ5+β-Co_5Ge_3, $Co_{11}Zr_2$+$Co_{23}Zr_6$+(α-Co), were not determined directly, they could be reasonably deduced in light of their adjacent two-phase regions.

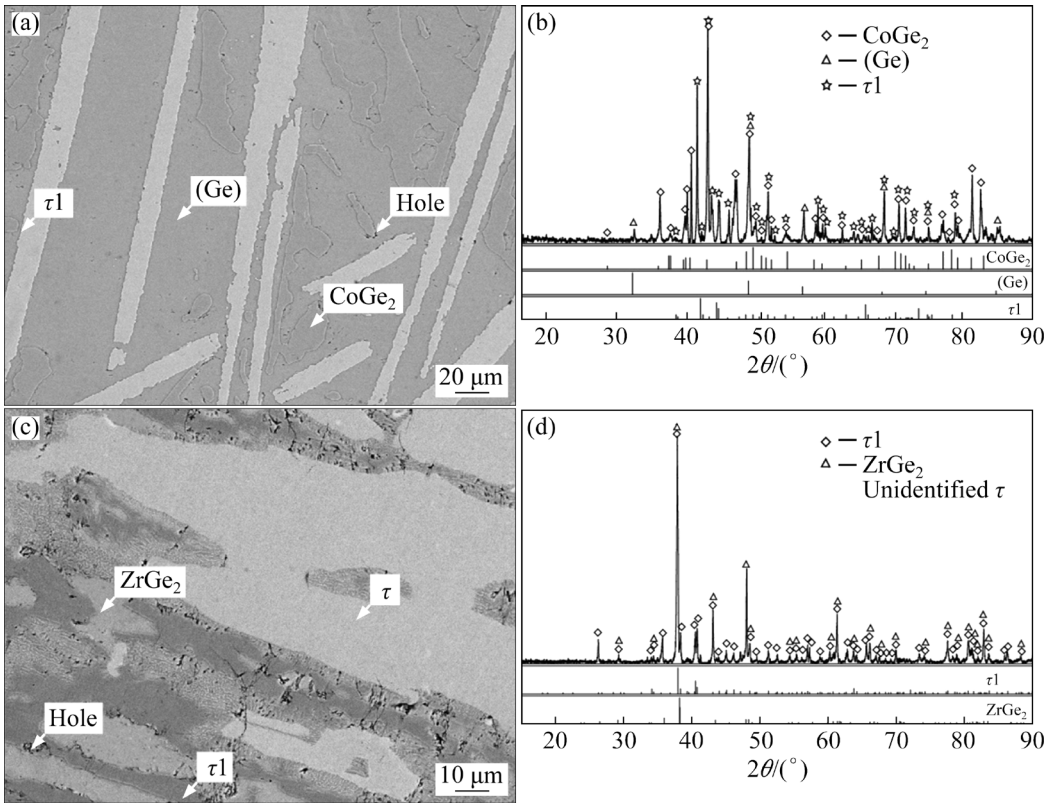

Fig. 3 BSE images (a, c) and XRD patterns (b, d) of typical alloys annealed at 1023 K for 90 d: (a, b) Alloy A16; (c, d) Alloy A20

Table 2 Constituent phases in Zr−Co−Ge alloys after annealing at 1023 K for 90 d

Alloy No.	Composition	Phase equilibrium	Phase composition/at.%								
		Phase 1/Phase 2/Phase 3	Phase 1			Phase 2			Phase 3		
			Zr	Co	Ge	Zr	Co	Ge	Zr	Co	Ge
A1	$Zr_{51}Co_{35}Ge_{14}$	CoZr/Zr_5Ge_3/Co_2Zr	50.1	49.2	0.7	62.3	3.1	34.6	34.4	62.3	3.3
A2	$Zr_{62}Co_{14}Ge_{24}$	CoZr/$CoZr_2$/Zr_5Ge_3	49.7	50.0	0.3	66.7	30.4	2.9	63.0	2.1	34.9
A3	$Zr_{55}Co_4Ge_{41}$	τ1/Zr_5Ge_3/Zr_5Ge_4	33.8	34.1	32.1	60.8	0.8	38.4	57.0	0.6	42.4
A4	$Zr_{72}Co_{23}Ge_5$	Zr_3Ge/$CoZr_3$/$CoZr_2$	74.7	2.1	23.2	73.9	26.0	0.1	66.6	31.8	1.6
A5	$Zr_{80}Co_{10}Ge_{10}$	(α-Zr)/$CoZr_3$/Zr_3Ge	99.6	0.3	0.1	74.5	25.4	0.1	75.9	1.5	22.5
A6	$Zr_{37}Co_{42}Ge_{21}$	Co_2Zr/τ4/Zr_5Ge_3	33.3	62.5	4.2	33.5	35.6	30.9	62.1	2.0	35.9
A7	$Zr_{43}Co_5Ge_{52}$	τ/$ZrGe_2$/ZrGe	44.1	14.7	41.2	33.4	0.5	66.0	50.5	0.3	49.2
A8	$Zr_{50}Co_9Ge_{41}$	τ/τ4/Zr_5Ge_4	41.0	19.4	39.6	33.8	33.8	32.4	55.3	1.5	43.2
A9	$Zr_{27}Co_{67}Ge_6$	$Co_{23}Zr_6$/Co_2Zr	21.1	71.0	7.9	27.6	68.7	3.7	–	–	–
A10	$Zr_{26}Co_{45}Ge_{29}$	τ2/τ4/τ5	18.9	56.4	24.7	34.0	34.5	31.5	24.2	42.8	33.0
A11	$Zr_{28}Co_{31}Ge_{41}$	τ5/τ4/τ1	27.5	37.6	34.9	33.4	34.3	32.3	27.6	29.0	43.4
A12	$Zr_{20}Co_{38}Ge_{42}$	τ3/τ1/τ5	7.6	47.9	44.5	26.6	28.4	45.0	26.4	38.6	35.0
A13	$Zr_{15}Co_{65}Ge_{20}$	(α-Co)/$Co_{23}Zr_6$/(ε-Co)	0.3	96.7	3.0	19.8	59.9	20.3	0.1	89.9	10.0
A14	$Zr_{15}Co_{47}Ge_{38}$	τ5/τ3/β-Co_5Ge_3	23.4	43.2	33.4	6.6	49.9	43.5	0.1	64.7	35.2
A15	$Zr_4Co_{94}Ge_2$	$Co_{23}Zr_6$/(α-Co)/$Co_{11}Zr_2$	20.6	67.5	12.0	0.2	99.4	0.4	12.9	81.8	5.3
A16	$Zr_9Co_{15}Ge_{76}$	$CoGe_2$/(Ge)/τ1	0.1	34.0	65.9	0.0	1.3	98.7	25.5	26.3	48.2
A17	$Zr_{17}Co_5Ge_{78}$	τ1/(Ge)/$ZrGe_2$	25.6	25.4	49.0	0.1	1.0	98.9	32.7	0.8	66.5
A18	$Zr_3Co_{52}Ge_{45}$	τ3/β-Co_5Ge_3/CoGe	5.5	48.5	46.0	0.0	59.6	40.4	1.0	51.8	47.2
A19	$Zr_{32}Co_{14}Ge_{54}$	τ1/$ZrGe_2$/τ	28.5	27.6	44.0	33.3	1.0	65.7	43.9	13.9	42.2
A20	$Zr_{38}Co_{10}Ge_{52}$	τ1/$ZrGe_2$/τ	28.3	27.9	43.7	33.6	1.7	64.7	44.1	13.8	42.1
A21	$Zr_8Co_{63}Ge_{29}$	β-Co_5Ge_3/τ2/(ε-Co)	1.0	65.0	34.0	17.5	56.3	26.2	0.1	82.4	17.5
A22	$Zr_8Co_{35}Ge_{57}$	τ1/τ3/$CoGe_2$	25.2	27.5	47.3	6.8	47.1	46.1	1.0	34.4	64.6

Ternary phases: τ1 ($Zr_4Co_4Ge_7$), τ2 ($Zr_6Co_{16}Ge_7$), τ3 ($ZrCo_6Ge_6$), τ4 (ZrCoGe), and τ5 ($Zr_4Co_7Ge_6$)

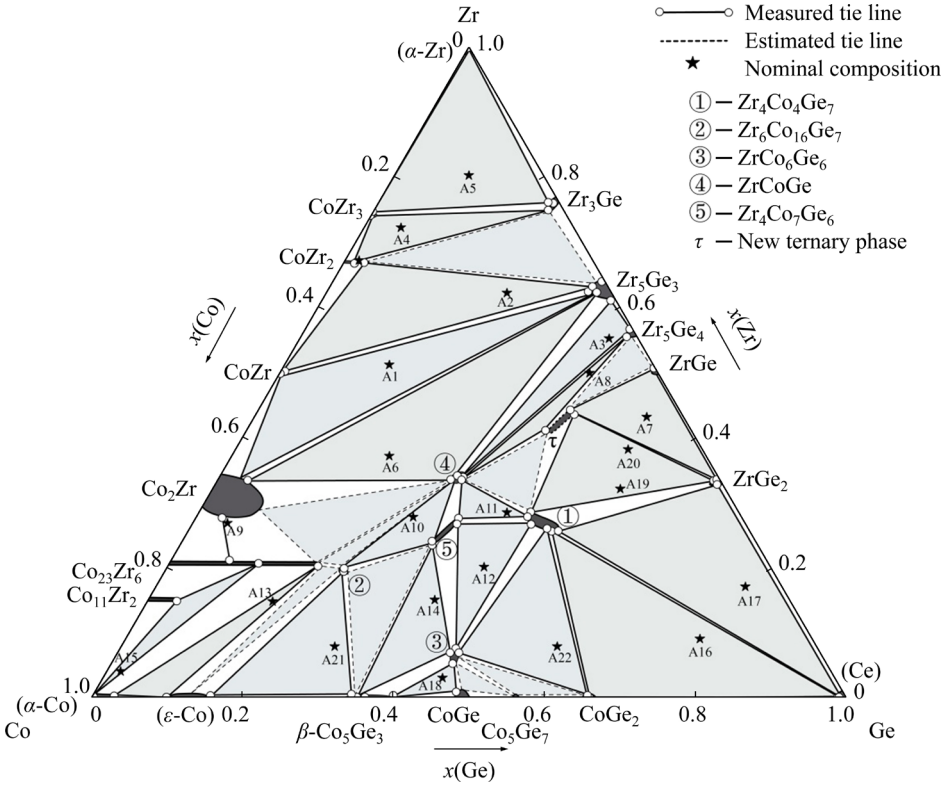

Fig. 4 Isothermal section of Zr−Co−Ge ternary system at 1023 K

3.2 Phase equilibria at 1173 K

The isothermal section of the Zr−Co−Ge system at 1173 K was further measured. Different annealed samples (B1−B24) have been supplied to determine the coexisting phases, which are summarized in Table 3. The microstructure of Alloy B9 with a nominal composition of $Zr_{37}Co_{42}Ge_{21}$ in BSE is elucidated in Fig. 5(a) along with XRD analyses (see Fig. 5(b)). It is noted that Alloy B9 comprises white Zr_5Ge_3, dark gray Co_2Zr, and gray $\tau4$. Based on the EPMA−WDS analysis in Fig. 5(c), Alloy B21 contains three phases, i.e., β-Co_5Ge_3, (ε-Co), and $\tau2$, in conformity with the result of XRD. Therefore, considering the alloy's nominal composition, Alloy B9 should lie in a three-phase area, Zr_5Ge_3+Co_2Zr+$\tau4$, while Alloy B21 lies in β-Co_5Ge_3+(ε-Co)+$\tau2$ instead.

In regards to Figs. 6(a) and (b) for Alloy B16, the ternary compounds, i.e., grey $\tau3$ and white $\tau1$, can be easily recognized, and eutectic structure consisting of solution phases ($CoGe_2$) and (Ge) could be further distinguished in the magnified image area. It should be noticed that this eutectic structure was the product of the liquid. According to the Co−Ge binary system [20], the eutectic reaction Liquid→($CoGe_2$)+(Ge) may happen when

Table 3 Constituent phases in Zr−Co−Ge alloys after annealing at 1173 K for 60 d

Alloy No.	Composition	Phase equilibrium	Phase composition/at.%								
		Phase 1/Phase 2/ Phase 3	Phase 1			Phase 2			Phase 3		
			Zr	Co	Ge	Zr	Co	Ge	Zr	Co	Ge
B1	$Zr_{23}Co_{50}Ge_{27}$	$Zr_3Ge/CoZr_3/(\beta$-Zr)	75.2	1.0	23.8	74.0	25.8	0.2	97.6	1.9	0.5
B2	$Zr_{43}Co_5Ge_{52}$	τ/ZrGe/$ZrGe_2$	42.2	12.9	44.9	47.0	0.4	52.6	31.6	1.0	67.3
B3	$Zr_{62}Co_{14}Ge_{24}$	$Zr_5Ge_3/CoZr_2/CoZr$	61.2	2.8	36.0	65.7	25.8	8.5	49.1	50.5	0.4
B4	$Zr_{72}Co_{22}Ge_6$	$Zr_3Ge/CoZr_2/CoZr_3$	74.0	24.6	1.4	65.3	18.2	16.4	73.7	0.9	25.4
B5	$Zr_{51}Co_{35}Ge_{14}$	$Zr_5Ge_3/Co_2Zr/CoZr$	60.6	2.5	36.9	34.3	61.6	4.2	49.1	47.3	3.5
B6	$Zr_{55}Co_4Ge_{41}$	$\tau4/Zr_5Ge_4/Zr_5Ge_3$	33.4	32.2	34.4	54.5	0.5	45.0	57.5	1.5	41.0
B7	$Zr_{32}Co_{14}Ge_{54}$	τ/$ZrGe_2$/$\tau4$	39.5	19.0	41.5	63.8	3.9	33.2	33.0	33.2	33.8
B8	$Zr_{50}Co_4Ge_{46}$	Zr_5Ge_4/τ/ZrGe	53.6	0.3	46.1	42.1	13.6	44.3	47.9	0.2	51.9
B9	$Zr_{37}Co_{42}Ge_{21}$	$Zr_5Ge_3/\tau4/Co_2Zr$	58.4	2.7	38.9	32.4	33.9	33.7	32.3	63.0	4.7
B10	$Zr_{26}Co_{69}Ge_5$	$Co_2Zr/Co_{23}Zr_6$	20.5	70.4	9.1	26.6	69.0	4.4	−	−	−
B11	$Zr_{20}Co_{38}Ge_{42}$	$\tau3/\tau1/\tau5$	7.0	46.6	46.4	25.4	27.4	47.2	22.4	41.5	36.1
B12	$Zr_{21}Co_{30}Ge_{49}$	$\tau1/\tau3$	24.2	25.5	50.3	6.7	46.7	46.6	−	−	−
B13	$Zr_{15}Co_{47}Ge_{38}$	$\tau5/\beta$-$Co_5Ge_3/\tau3$	22.1	42.5	35.3	0.0	62.3	37.6	7.3	47.4	45.2
B14	$Zr_{17}Co_5Ge_{78}$	$\tau1$/$ZrGe_2$/(Ge)	23.4	25.3	51.3	31.2	1.3	67.5	0.0	2.5	97.5
B15	$Zr_{19}Co_{49}Ge_{32}$	$\tau1/\tau5/\beta$-Co_5Ge_3	18.7	54.4	26.9	21.9	42.4	35.7	0.1	65.2	34.7
B16*	$Zr_8Co_{35}Ge_{57}$	$\tau3/\tau1$/Liquid	6.8	47.0	46.2	23.2	26.1	50.7	0.0	33.9	66.1
B17	$Zr_{10}Co_{80}Ge_{10}$	(ε-Co)/$Co_{23}Zr_6/\tau4$	0.0	97.4	2.6	20.0	61.7	18.3	32.5	34.5	33.0
B18	$Zr_3Co_{51}Ge_{46}$	β-$Co_5Ge_3/\tau3$/CoGe	0.0	57.7	42.3	4.7	48.3	47.0	0.0	50.3	49.6
B19	$Zr_4Co_{94}Ge_2$	$Co_{23}Zr_6/(\alpha$-Co)	21.1	72.8	6.1	0.0	99.1	0.9	−	−	−
B20	$Zr_{19}Co_{61}Ge_{20}$	$\tau4/\tau2/(\varepsilon$-Co)	33.1	34.2	32.7	19.3	57.5	23.2	1.2	92.7	6.1
B21	$Zr_8Co_{63}Ge_{29}$	$\tau2/\beta$-$Co_5Ge_3/(\alpha$-Co)	18.5	54.3	27.2	0.0	65.8	34.2	0.0	82.6	17.4
B22	$Zr_{30}Co_{28}Ge_{42}$	$ZrGe_2/\tau4/\tau1$	32.1	3.8	64.1	32.7	33.5	33.8	26.8	27.5	45.7
B23	$Zr_{38}Co_{23}Ge_{39}$	$Zr_5Ge_4/\tau4/\tau$	54.6	0.8	44.6	33.1	33.0	33.9	43.5	13.1	43.4
B24	$Zr_{28}Co_{31}Ge_{41}$	$\tau4/\tau1/\tau5$	31.4	34.6	34.0	25.9	28.6	45.5	24.7	39.6	35.7

Ternary phases: $\tau1$ ($Zr_4Co_4Ge_7$), $\tau2$ ($Zr_6Co_{16}Ge_7$), $\tau3$ ($ZrCo_6Ge_6$), $\tau4$ (ZrCoGe), and $\tau5$ ($Zr_4Co_7Ge_6$).

* The composition of the Liquid phase can be reasonably estimated

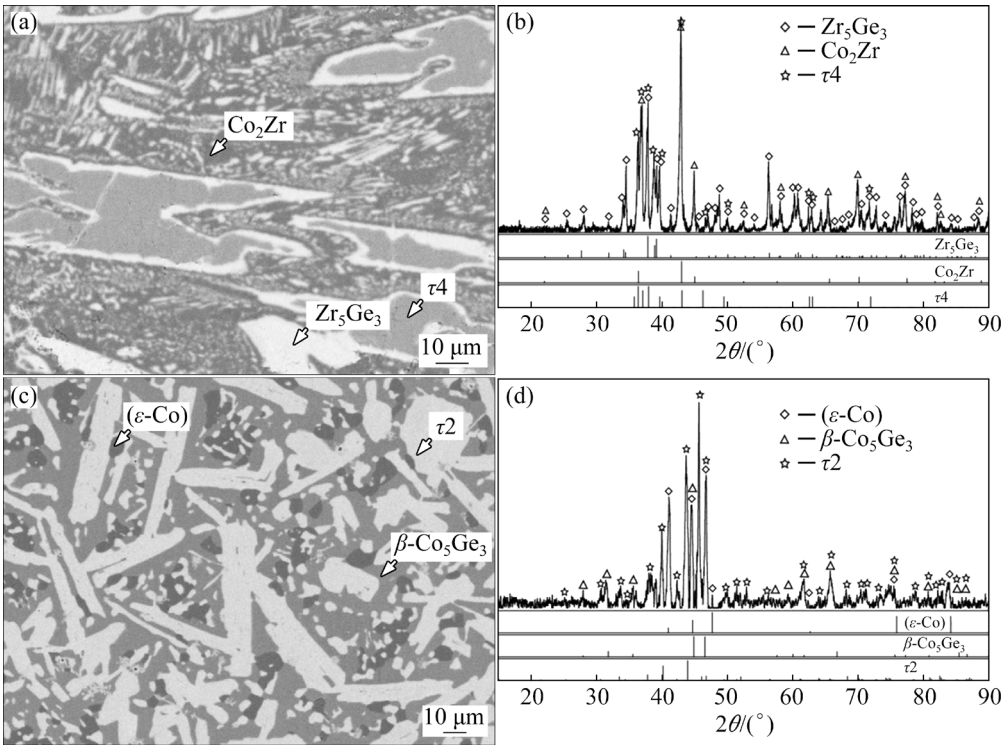

Fig. 5 BSE images (a, c) and XRD patterns (b, d) of typical alloys annealed at 1173 K for 60 d: (a, b) Alloy B9; (c, d) Alloy B21

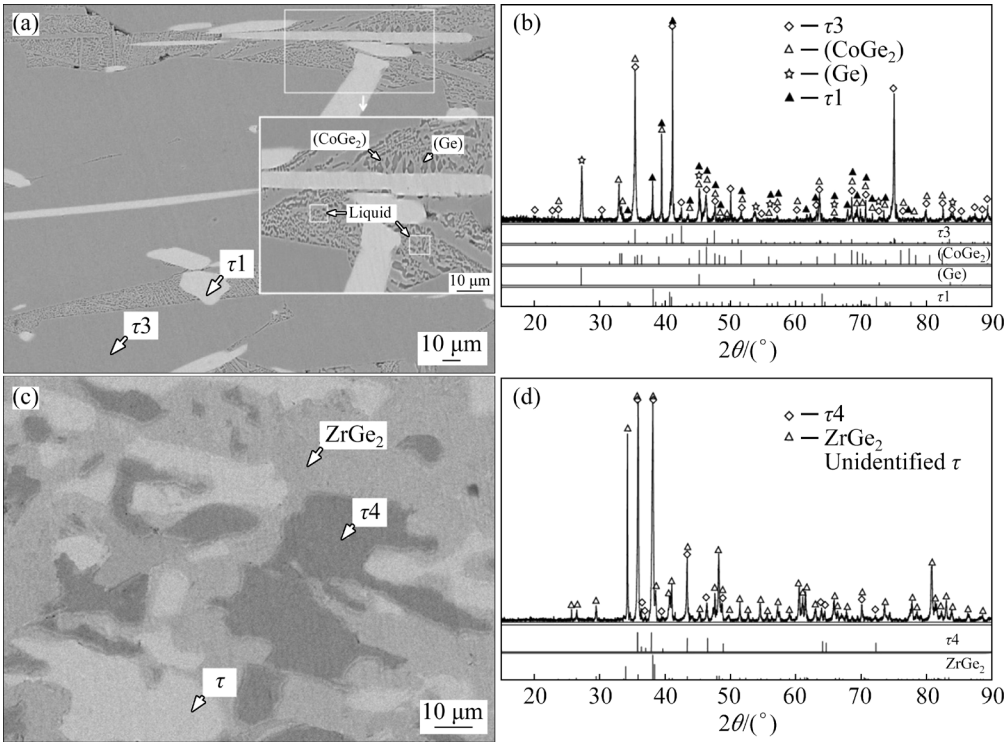

Fig. 6 BSE images (a, c) and XRD patterns (b, d) of typical alloys annealed at 1173 K for 60 d: (a, b) Alloy B16; (c, d) Alloy B7

the liquid with composition close to the binary eutectic reaction was cooled. When the ternary alloy such as B16 was homogenized at 1173 K, the liquid should be formed as a phase in equilibrium with other phases and transformed into ($CoGe_2$) and (Ge) during cooling later. Briefly, the actual phase

equilibrium in Alloy B16 should be $\tau 3+\tau 1+$Liquid. By the way, the composition of the liquid phase in Alloy B16 was reasonably regarded as the average of the eutectic structure ($CoGe_2$)+(Ge).

As illustrated in Figs. 6(c) and (d), Alloy B7 involved 3 phases, i.e., $ZrGe_2$, $\tau 4$, and another new phase with the composition of 39.5Zr−19.0Co−41.5Ge (at.%). The composition of this new phase in Alloy B7 was close to that of the τ phase in Alloy A20. By further comparing the characteristic diffraction peaks of this new phase in Alloy B7 with those of the τ phase in Alloy A20, it was considered that the unidentified phases in Alloys B7 and A20 were the same phase. Therefore, the significant three-phase equilibrium $ZrGe_2+\tau 4+\tau$ was reasonably determined.

On the grounds of the experimental results achieved in this study, the isothermal section of the Zr−Co−Ge ternary system at 1173 K has been built, as displayed in Fig. 7, where 28 three-phase regions were discovered. Among several marked ternary phases, a new ternary phase τ was reliably detected with the contents of 39.5−43.5 at.% Zr, 12.9−19.0 at.% Co and 41.5−44.9 at.% Ge at 1173 K. Besides, the third element shows limited solubility in $CoZr_2$, Co_2Zr, $Co_{23}Zr_6$, and Zr_5Ge_3.

3.3 Phase equilibria at 1373 K

Typical annealed alloys were prepared to establish the isothermal section of the Zr−Co−Ge ternary system at 1373 K. The phases coexisting in the homogenized alloys were summarized in Table 4. Figure 8(a) presented the BSE images of Alloy C5 with the nominal composition of $Zr_{37}Co_{42}Ge_{21}$. Distinct coexistence of three phases, i.e., the white Zr_5Ge_3, dark Co_2Zr, and gray ternary compound $\tau 4$, were found, in synchronization with the result of XRD shown in Fig. 8(b). Comparably, through EPMA−WDS assisted with XRD analysis (see Figs. 8(c) and (d)), white $Co_{23}Zr_6$, gray $Co_{11}Zr_2$, and dark (α-Co) were expressly discerned in Alloy C19. Consequently, phase equilibria of $Zr_5Ge_3+Co_2Zr+\tau 4$ and $Co_{23}Zr_6+Co_{11}Zr_2+(\alpha$-Co) were capable of being discriminated in Alloys C5 and C19 at 1373 K, respectively.

In light of the Co−Ge binary diagram, liquid can be formed in the Co−Ge alloys at the estimated composition of 49−100 at.% Ge at 1373 K [20]. Notwithstanding, it is difficult to get the well-equilibrated microstructure characteristic referring to the alloy of the inclusive liquid phase after annealing at a high temperature of 1373 K, the correlative phase relations were still significant,

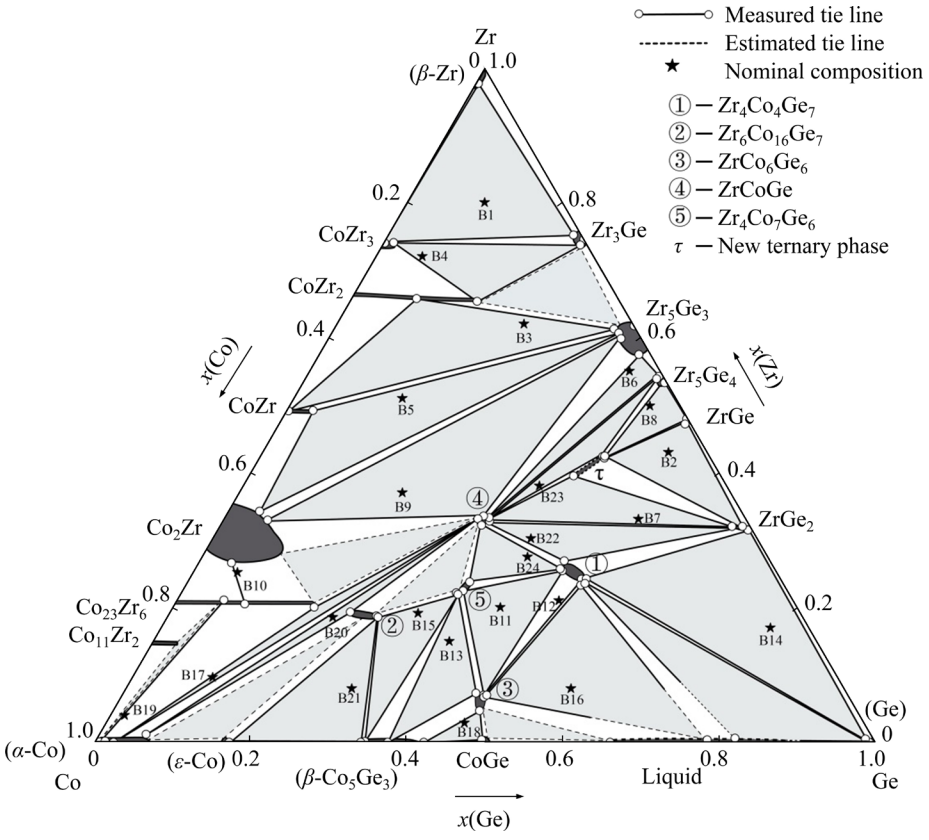

Fig. 7 Isothermal section of Zr−Co−Ge ternary system at 1173 K

Table 4 Constituent phases in Zr−Co−Ge alloys after annealing at 1373 K for 10 d

Alloy No.	Composition	Phase equilibrium	Phase composition/at.%								
		Phase 1/Phase 2/Phase 3	Phase 1			Phase 2			Phase 3		
			Zr	Co	Ge	Zr	Co	Ge	Zr	Co	Ge
C1	$Zr_{62}Co_{14}Ge_{24}$	$CoZr_2/CoZr/Zr_5Ge_3$	66.3	21.5	12.2	50.0	49.3	0.7	62.5	2.3	35.2
C2	$Zr_{55}Co_4Ge_{41}$	$Zr_5Ge_4/Zr_5Ge_3/\tau4$	53.9	0.4	45.7	59.2	0.7	40.1	32.5	32.6	34.9
C3	$Zr_{90}Co_2Ge_8$	$Zr_3Co/(\beta$-Zr)	75.6	1.3	23.1	99.8	0.1	0.1	−	−	−
C4	$Zr_{51}Co_{35}Ge_{14}$	$CoZr/Zr_5Ge_3/Co_2Zr$	48.6	49.3	2.1	60.5	1.7	37.8	32.7	62.5	4.8
C5	$Zr_{37}Co_{42}Ge_{21}$	$Zr_5Ge_3/Co_2Zr/\tau4$	59.8	2.1	38.1	32.2	60.3	7.5	32.3	34.1	33.6
C6*	$Zr_{80}Co_{10}Ge_{10}$	$Zr_3Ge/CoZr_2$/Liquid	74.1	1.5	24.4	65.3	11.9	22.8	73.6	24.0	2.4
C7*	$Zr_{23}Co_{50}Ge_{27}$	$Zr_3Ge/(\beta$-Zr)/Liquid	73.8	1.6	24.6	74.8	23.7	1.5	88.4	10.3	1.3
C8	$Zr_{19}Co_{61}Ge_{20}$	$(\alpha$-Co)/$Co_{23}Zr_6/\tau2$	0.0	95.7	4.3	19.8	62.7	17.5	20.1	57.3	22.6
C9*	$Zr_{17}Co_5Ge_{78}$	$ZrGe_2$/Liquid	31.6	0.8	67.6	0.1	16.7	83.2	−	−	−
C10*	$Zr_9Co_{22}Ge_{68}$	$\tau1$/Liquid	23.9	25.9	50.2	0.3	19.1	80.6	−	−	−
C11*	$Zr_{25}Co_{17}Ge_{58}$	$\tau1/ZrGe_2$/Liquid	24.5	26.4	49.1	31.5	2.3	66.2	2.1	18.1	80.8
C12	$Zr_{28}Co_{45}Ge_{27}$	$Co_2Zr/\tau4/Co_{23}Zr_6$	24.9	59.0	16.1	32.9	34.0	33.0	20.7	62.7	17.5
C13	$Zr_{15}Co_{47}Ge_{38}$	$\tau5/\tau3/Co_5Ge_3$	21.9	42.4	35.7	7.2	47.8	45.0	0.0	62.9	37.0
C14	$Zr_{32}Co_{14}Ge_{54}$	$\tau4/ZrGe_2/\tau$	32.2	32.9	34.9	31.6	2.6	65.8	41.6	14.9	43.5
C15*	$Zr_8Co_{35}Ge_{57}$	Liquid/$\tau1/\tau3$	0.5	30.3	69.2	23.2	27.3	49.5	7.0	45.2	47.8
C16	$Zr_{50}Co_3Ge_{47}$	$Zr_5Ge_4/ZrGe/\tau$	52.2	0.1	47.6	48.2	0.2	51.6	41.2	13.3	45.5
C17	$Zr_{43}Co_5Ge_{52}$	$ZrGe_2/\tau/ZrGe$	31.2	2.0	66.8	42.0	12.3	45.7	48.7	0.0	51.3
C18	$Zr_{23}Co_{72}Ge_5$	$Co_2Zr/Co_{23}Zr_6$	23.6	71.7	4.6	20.5	72.8	6.8	−	−	−
C19	$Zr_{10}Co_{82}Ge_8$	$(\alpha$-Co)/$Co_{11}Zr_2/Co_{23}Zr_6$	0.1	96.5	3.4	14.8	76.5	8.6	19.8	63.1	17.1
C20	$Zr_{20}Co_{38}Ge_{42}$	$\tau1/\tau3/\tau5$	22.4	41.8	35.8	7.2	46.1	46.7	24.7	27.8	47.5
C21	$Zr_{25}Co_{45}Ge_{30}$	$\tau5/\tau2/\tau4$	23.0	41.3	35.7	20.1	55.1	24.8	31.4	34.0	34.6
C22	$Zr_{21}Co_{48}Ge_{31}$	β-$Co_5Ge_3/\tau5/\tau2$	0.2	63.6	36.2	22.1	42.4	35.5	19.8	55.8	24.4
C23	$Zr_{30}Co_{28}Ge_{42}$	$\tau1/ZrGe_2/\tau4$	25.8	27.4	46.8	31.1	2.4	66.5	31.7	33.1	35.2
C24*	$Zr_3Co_{52}Ge_{45}$	$\tau3$/Liquid/β-Co_5Ge_3	5.0	49.1	45.9	0.0	51.0	49.0	0.0	58.1	41.9
C25	$Zr_{18}Co_{73}Ge_9$	$Co_{11}Zr_2/Co_{23}Zr_6$	15.6	77.2	7.3	19.6	65.4	15.0	−	−	−
C26	$Z_{44}Co_{11}Ge_{45}$	$Zr_5Ge_4/\tau4/\tau$	53.2	0.4	46.4	35.0	32.0	33.0	44.0	42.3	13.7
C27	$Zr_8Co_{63}Ge_{29}$	β-$Co_5Ge_3/(\varepsilon$-Co)/$\tau2$	0.0	64.4	35.6	0.5	83.1	16.4	19.6	57.2	23.2
C28	$Zr_{15}Co_{67}Ge_{18}$	$(\alpha$-Co)/$\tau2$	0.1	90.1	9.8	20.1	57.3	22.6	−	−	−

Ternary phases: $\tau1$ ($Zr_4Co_4Ge_7$), $\tau2$ ($Zr_6Co_{16}Ge_7$), $\tau3$ ($ZrCo_6Ge_6$), $\tau4$ (ZrCoGe), and $\tau5$ ($Zr_4Co_7Ge_6$).

* The composition of the Liquid phase can be reasonably estimated

and thereby a portion of samples were further investigated, e.g., C9, C10, and C15. Figure 9(a) offers a BSE micrograph of Alloy C9, of which the shapes and colors of constituent phases can be precisely detected. With the help of XRD, the white stick-shaped phase was $ZrGe_2$, and the typical eutectic microstructure contained the solution phase, i.e., gray (Ge) and dark gray ($CoGe_2$), in the magnified micrograph. Like Alloy B16, the regularly distributed ($CoGe_2$) and matrix (Ge) phases in Alloy C9 were most likely precipitated from the liquid during the quenching after the alloy was kept at 1373 K. Hence, the real phase equilibrium in Alloy C9 at 1373 K should be $ZrGe_2$ + Liquid, and another two-phase region, $\tau1$+ Liquid, occurred in Alloy C10 in similar manner.

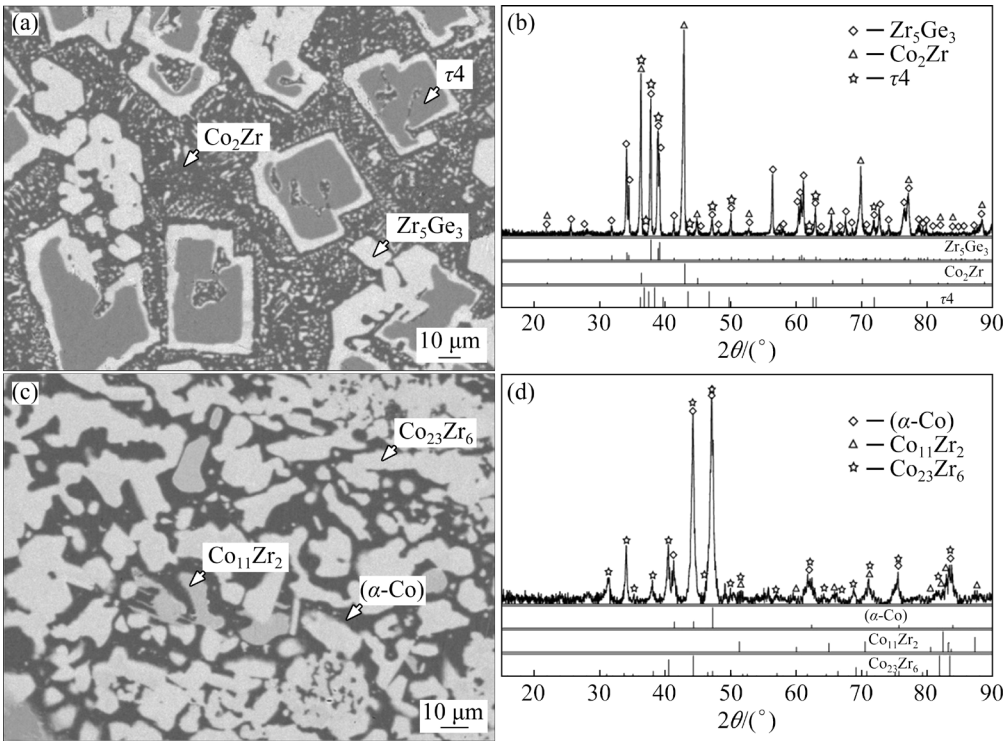

Fig. 8 BSE images (a, c) and XRD patterns (b, d) of typical alloys annealed at 1373 K for 10 d: (a, b) Alloy C5; (c, d) Alloy C19

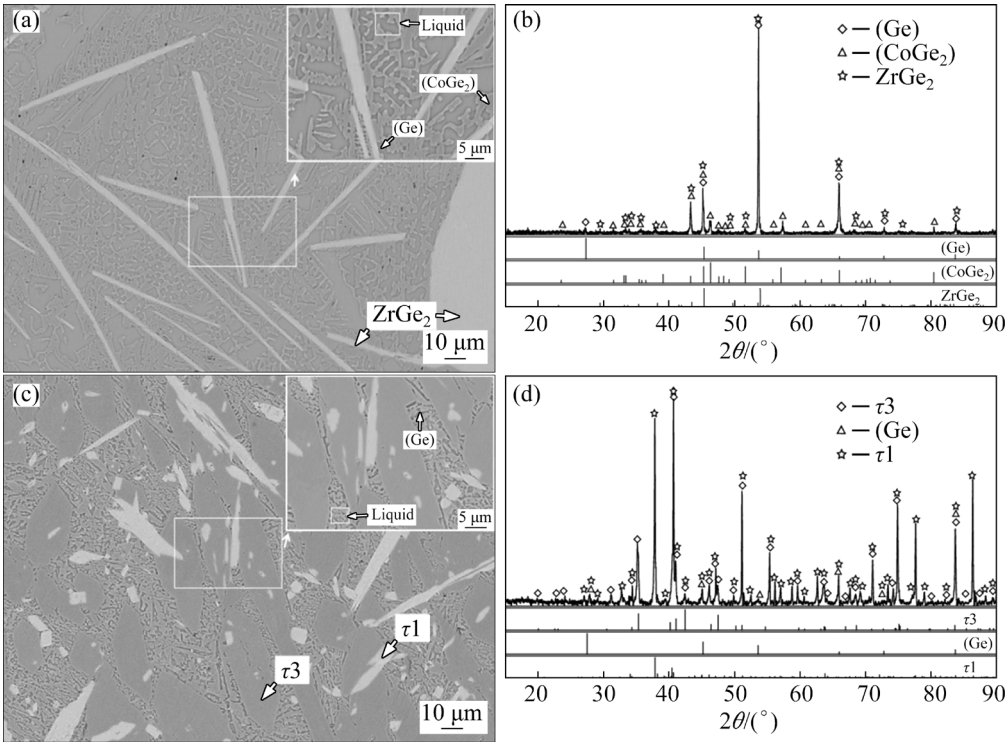

Fig. 9 BSE images (a, c) and XRD patterns (b, d) of including liquid phase alloys annealed at 1373 K for 10 d: (a, b) Alloy C9; (c, d) Alloy C15

Therefore, by combining Alloys C9 with C10, the three-phase region $ZrGe_2$+τ1+Liquid could be legitimately inferred. The coexistence of the three phases in Alloy C15, solution (Ge), ternary compounds τ1 and τ3, were identified by using EPMA−WDS and XRD (as illustrated in Figs. 9(c)

and (d)). Differing from Alloy C9, the solution phase (Ge) may primarily solidify from the liquid phase and followed by the formation of the eutectic microstructure (Ge)+τ3 during cooling. So, the corresponding phase equilibrium in Alloy C15 was considered to be τ1+ τ3+Liquid.

Similar to the case of Alloy B7, the τ phase and the other two phases τ4 and $ZrGe_2$ were also detected in Alloy C14, as shown in Fig. 10. τ in Alloy C14 is with the composition of 41.6Zr−14.9Co−43.5Ge (at.%). Here, the three-phase field of $ZrGe_2$+τ4+τ was determined. Based on Table 4, the isothermal section at 1373 K of the Zr−Co−Ge system was measured as stated in Fig. 11, where 26 three-phase regions were achieved, and the composition of the reported ternary phases was ulteriorly confirmed. Additionally, the new ternary phase τ, revealed a specific composition range, i.e., 41.2−42.0 at.% Zr and 12.3−14.9 at.% Co. It is of the utmost importance to acquire the crystallographic information and stability of the new τ phase. However, after trying many times, we failed to prepare the single-phase sample by casting and annealing methods and so failed to collect the X-ray patterns of τ further. The phase τ could not be synthesized via crystal growth from the liquid.

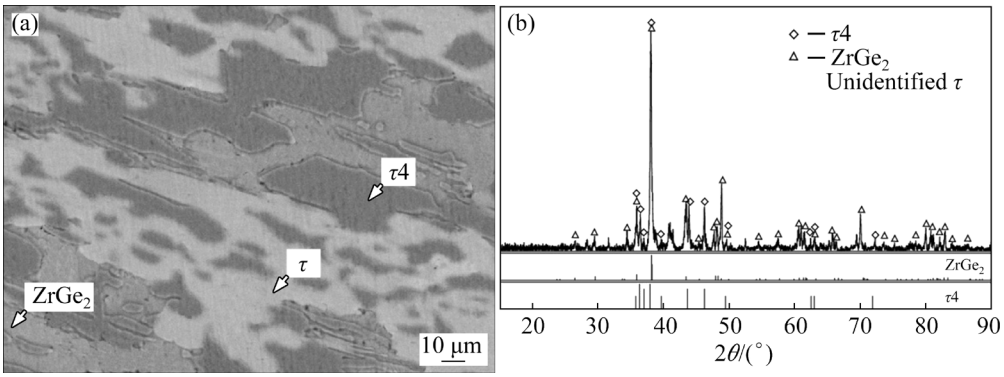

Fig. 10 Constituent phases in Alloy C14 annealed at 1173 K for 60 d: (a) BSE; (b) XRD pattern

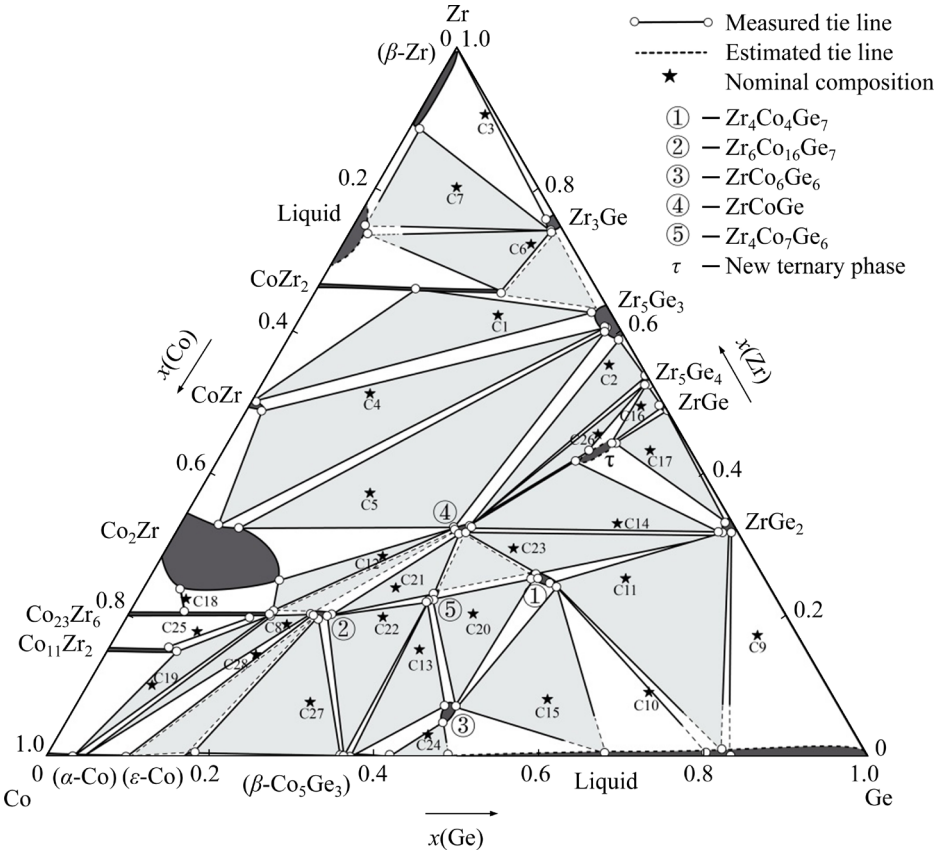

Fig. 11 Isothermal section of Zr−Co−Ge ternary system at 1373 K

3.4 Comparison of phase equilibria at 1023, 1173, and 1373 K

Phase equilibria in the Zr−Co−Ge ternary system at 1023, 1173, and 1373 K were compared here. As illustrated in Figs. 3, 5, and 8, some distinct differences between these three isothermal sections are presented.

Firstly, it is noteworthy that the three-phase equilibria of τ+τ1+τ4 and τ+τ1+$ZrGe_2$ at 1023 K change to τ+$ZrGe_2$+τ4 and τ4+τ1+$ZrGe_2$ at 1173 K. This implies that an invariant reaction, τ+τ1$\rightleftharpoons$$\tau$4+$ZrGe_2$, occurs at a temperature between 1023 and 1173 K. To further check the phase transitions in Alloys C14, B7 and A19 of the same nominal composition ($Zr_{32}Co_{14}Ge_{54}$) concerning the τ, τ1, τ4, and $ZrGe_2$ phases, a simple verification was conducted and thus the phase transition was demonstrated. As revealed in Figs. 12(a) and (b), the annealed Alloy C14 re-annealed at 1073 and 1023 K for 5 d was carried out, denoted as Alloys D1 and D2, respectively. Four distinct non-equilibrated phases, i.e., white τ of composition 38.9Zr−18.7Co−42.4Ge, gray τ1 of composition 26.2Zr−26.7Co−47.1Ge, dark gray τ4 of 32.4Zr−32.5Co−35.1Ge and light gray $ZrGe_2$ of 31.1Zr−2.8Co−66.1Ge (at.%) can be observed in Fig. 12(a), in accordance with the XRD result in Fig. 12(c) except for the unidentified new phase τ. It is noted that the amount of τ4 in Alloy D1 decreases while that of τ1 increases, in comparison with Alloy D2 annealed at 1023 K for 5 d in Fig. 12(b). In other words, phase transition must happen in Alloy C14 at a specific temperature, and the relevant verification will be done in future work.

Secondly, the new ternary phase τ is initially detected for the first time. τ exhibits a wide homogeneity range altering from 41.0−44.1 at.% Zr and 13.8−19.4 at.% Co at 1023 K to 39.5−43.5 at.% Zr and 12.9−19.0 at.% Co at 1173 K and to 41.2−42.0 at.% Zr and 12.3−14.9 at.% Co at 1373 K, indicating that it can be tuned by changing Zr or Co content in a relatively wide range. Measurement of crystal structure and stability of τ is in progress.

Thirdly, due to the appearance of liquid phase, the phase relations among τ1, τ3, $CoGe_2$ and (Ge) have been respectively described, which transform from τ1+τ3+$CoGe_2$ and τ1+$CoGe_2$+(Ge) at 1023 K, to τ1+τ3+Liquid and τ1+Liquid+(Ge) at 1173 K, and to τ1+τ3+Liquid and τ1+Liquid at 1373 K.

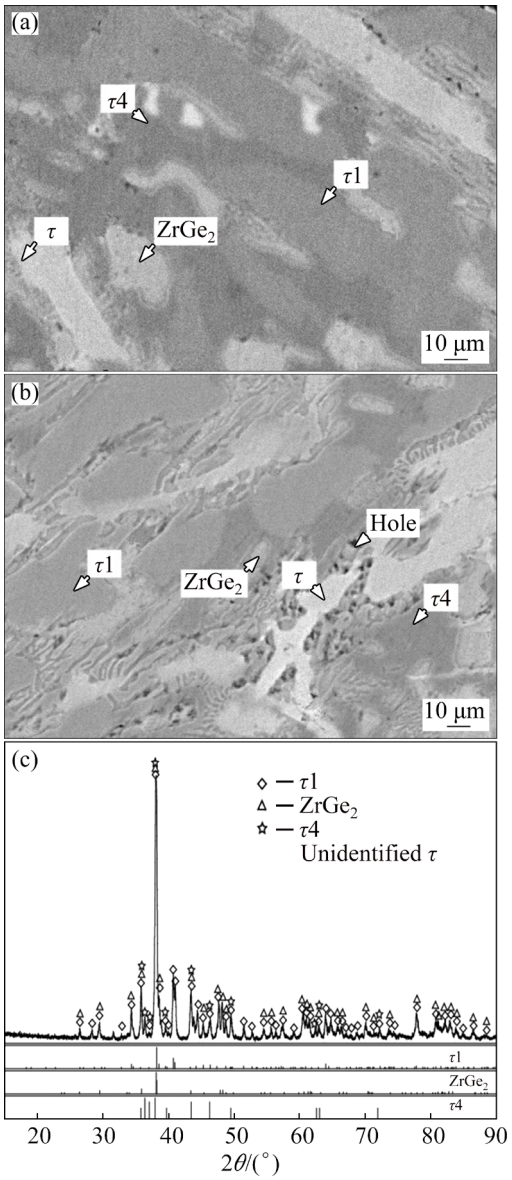

Fig. 12 BSE images of Alloy D1 annealed at 1073 K for 5 d (a), BSE image of Alloy D2 annealed at 1023 K for 5 d (b), and XRD pattern of Alloy D1 annealed at 1073 K for 5 d (c)

Last but not the least, alloy element Ge can substitute Co for certain content in some Co−Zr phases. For instance, Ge can substitute for about 22.8 at.%, 16.4 at.% and 2.9 at.% Co in $CoZr_2$ phase, and 20.3 at.%, 18.3 at.% and 17.5 at.% Co in $Co_{23}Zr_6$ phase at 1023, 1173 and 1373 K, respectively.

4 Conclusions

(1) Combined with the EPMA and XRD techniques, 29, 28 and 26 three-phase regions have

been respectively determined in the Zr−Co−Ge ternary system at 1023, 1173 and 1373 K.

(2) Six ternary phases have been observed and the related composition ranges have been identified, of which a new ternary phase τ is first detected with a wide homogeneity area of 41.0−44.1 at.% Zr and 13.8−19.4 at.% Co at 1023 K, to 39.5−43.5 at.% Zr and 12.9−19.0 at.% Co at 1173 K, and to 41.2−42.0 at.% Zr and 12.3−14.9 at.% Co at 1373 K.

(3) Between 1023 and 1173 K, the three-phase regions $\tau+\tau1+\tau4$ and $\tau+\tau1+ZrGe_2$ at 1023 K change to $\tau+ZrGe_2+\tau4$ and $\tau4+\tau1+ZrGe_2$ at 1173 K, showing that an invariant transition of $\tau+\tau1 \rightleftharpoons \tau4+ZrGe_2$ is deduced.

References

[1] GUO G H, QIN J, ZHANG H B. Magnetocrystalline anisotropy and spin reorientation transition of $DyMn_6Sn_6$ compound [J]. Transactions of Nonferrous Metals Society of China, 2007, 17: 514−518.

[2] QIE Y Q, LIU Y X, KONG F Q, SHI Z, YANG H. Hard magnetic cobalt nanomaterials as an electrocatalyst for oxygen evolution reaction [J]. Journal of Materials Science: Materials in Electronics, 2021, 32: 17490−17499.

[3] STROINK G, STADNIK Z M, VIAU G, DUNLAP R A. The influence of quenching rate on the magnetic properties of microcrystalline alloys $Co_{80}Zr_{20-x}B_x$ [J]. Journal of Applied Physics, 1990, 67: 4963−4965.

[4] STRNAT K J, STRNAT R M W. Rare earth-cobalt permanent magnets [J]. Journal of Magnetism and Magnetic Materials, 1991, 100: 38−56.

[5] SAITO T. The origin of the coercivity in Co−Zr system alloys [J]. IEEE Transactions on Magnetics, 2003, 39: 2890−2892.

[6] SAITO T. Magnetization process in Co−Zr−B permanent-magnet materials [J]. IEEE Transactions on Magnetics, 2004, 40: 2919−2921.

[7] TOLEA F, PALADE P, SOFRONIE M, POPESCU B, KUNCSER V. Effect of Cr, C, B and Mo substitutions on the structure and magnetic properties of Zr−Co rare-earth-free magnetic alloy [J]. IOP Conference Series: Materials Science and Engineering, 2019, 485: 012028.

[8] WANG X T, CUI Y T, LIU X F, LIU G D. Electronic structures and magnetism in the Li_2AgSb-type Heusler alloys, Zr_2CoZ (Z=Al, Ga, In, Si, Ge, Sn, Pb, Sb): A first-principles study [J]. Journal of Magnetism and Magnetic Materials, 2015, 394: 50−59.

[9] ISHIKAWA T, OHMORI K. Hard magnetic phase in rapidly quenched Zr−Co−B alloys [J]. IEEE Transactions on Magnetics, 1990, 26: 1370−1372.

[10] HU K, DONG S S, SHEN C, LIU H S, PENG H L, CAI G M, JIN Z P. Measurement of phase equilibria in Ti−Co−Ge ternary system [J]. Journal of Alloys and Compounds, 2019, 793: 653−661.

[11] GABAY A M, ZHANG Y, HADJIPANAYIS G C. Cobalt-rich magnetic phases in Zr−Co alloys [J]. Journal of Magnetism and Magnetic Materials, 2001, 236: 37−41.

[12] MAO J F, HE L L, YE H Q, YANG D Z, TANG Z X. An HRTEM study of the crystal structure of $Zr_4Co_4Ge_7$ [J]. Materials Letters, 1994, 21: 307−312.

[13] LIU X J, ZHANG H H, WANG C P, ISHIDA K. Experimental determination and thermodynamic assessment of the phase diagram in the Co−Zr system [J]. Journal of Alloys and Compounds, 2009, 482: 99−105.

[14] DURGA A, HARI KUMAR K C. Thermodynamic optimization of the Co−Zr system [J]. Calphad, 2010, 34: 200−205.

[15] OKAMOTO H. Co−Zr (cobalt−zirconium) [J]. Journal of Phase Equilibria and Diffusion, 2011, 32: 169−170.

[16] SHA C S, ZHOU L C, LIU S H, DU Y, GANG T, XU H H. Phase equilibria and thermodynamic modeling in the Ge−Zr binary system [J]. Journal of Materials Science, 2011, 46: 1405−1413.

[17] OKAMOTO H. Ge−Zr (germanium−zirconium) [J]. Journal of Phase Equilibria and Diffusion, 2012, 33: 424.

[18] LIU Y X, YIN F C, LI Z, CHEN L P. Experimental determination of 800 ℃ isothermal section in Al−Zn−Zr ternary system [J]. Transactions of Nonferrous Metals Society of China, 2019, 29: 25−33.

[19] LÜ K L, YANG F, XIE Z Y, LIU H S, CAI G M, JIN Z P. Isothermal section of Al−Ti−Zr ternary system at 1073 K [J]. Transactions of Nonferrous Metals Society of China, 2016, 26: 3052−3058.

[20] ZENG Y P, LI H, DU Y, PAN Y F, PENG Y B, ZHOU P, PREMOVIC M. Experimental investigation of the Co−Ge phase diagram [J]. Journal of Phase Equilibria and Diffusion, 2017, 38: 843−852.

[21] ZENG Y P, DU Y, LI H, ZHOU P, LIU S H. Thermodynamic description and solidified microstructure of the Co−Ge system [J]. Journal of Alloys and Compounds, 2019, 793: 480−491.

[22] ENOKI H, ISHIDA K, NISHIZAWA T. Phase equilibria in cobalt-rich portions of the Co−Si and Co−Ge systems [J]. Journal of the Less Common Metals, 1990, 160: 153−160.

[23] TAKIZAWA H, SATO T, ENDO T, SHIMADA M. High-pressure synthesis and electrical and magnetic properties of MnGe and CoGe with the cubic B20 structure [J]. Journal of Solid State Chemistry, 1988, 73: 40−46.

[24] JEITSCHKO W. The crystal structure of $Zr_4Co_4Ge_7$ (V-phase) [J]. Acta Crystallographica, 1969, 25: 557−564.

[25] BUSCHOW K H J, VAN ENGEN P G, JONGEBREUR R. Magneto-optical properties of metallic ferromagnetic materials [J]. Journal of Magnetism and Magnetic Materials, 1983, 38: 1−22.

[26] BUCHHOLZ W, SCHUSTER H U. Intermetallische phasen mit B35-berstruktur und verwandtschafts-beziehung zu $LiFe_6Ge_6$ [J]. Zeitschrift für Anorganische und Allgemeine Chemie, 1981, 482: 40−48. (in Germany)

[27] JEITSCHKO W, JORDAN A G, BECK P A. V and E phases in ternary systems with transition metals and silicon or germanium [J]. Transactions of the Metallurgical Society of AIME, 1969, 245: 335−339.

[28] OLENYCH R R, YARMOLYUK Y P, SKOKOZDNE R V.

Magnetic susceptibility of the compounds Ti(Zr,Hf)Co_6Ge_6, Ti(Zr,Hf)$_4Co_7Ge_6$ and crystal structure of $Ti_4Co_7Ge_6$ [J]. Ukrainskii Fizicheskii Zhurnal, 1987, 32: 615−618.

[29] YOUSUF S, GUPTA D C. Chemical potential evaluation of thermoelectric and mechanical properties of Zr_2CoZ (Z=Si, Ge) Heusler alloys [J]. Journal of Electronic Materials, 2018, 47: 2468−2478.

[30] WEI X P, GAO P F, ZHANG Y L, ZHANG H B. Investigations on exchange interactions and Curie temperatures of Zr_2CoZ compounds by using first-principles and Monte Carlo calculations [J]. Journal of Magnetism and Magnetic Materials, 2019, 477: 190−197.

[31] YOUSUF S, GUPTA D C. Insight into mechanical properties and thermoelectric efficiency of Zr_2CoZ (Z=Si,Ge) Heusler alloys [J]. Materials Research Express, 2017, 4: 116307.

[32] LI L L, ZHANG J B, CHEN Y C, YANG S Y, WANG C P, LIU X J. Phase equilibria in Co−Al−Re ternary system at 1100 and 1300 ℃ [J]. Transactions of Nonferrous Metals Society of China, 2021, 31: 1740−1747.

[33] ANDRÉ D, PIERRE F. Les systèmes binaires cobalt-germanium et nickel-germanium Étude comparée [J]. Journal of the Less Common Metals, 1980, 72: 51−70. (in French)

[34] BUSCHOW K H J. Crystallization of amorphous $Zr_{1-x}Co_x$ alloys [J]. Journal of the Less Common Metals, 1982, 85: 221−231.

[35] BAILEY D M, SMITH J F. A note on the structure of Zr_2Co [J]. Acta Crystallographica, 1961, 14: 1084−1084.

[36] FUJII H, POURARIAN F, WALLACE W E. Appearance of spontaneous ferromagnetism in non-stoichiometric $ZrCo_2$ [J]. Journal of Magnetism and Magnetic Materials, 1981, 24: 93−96.

[37] IVANOVA G V, SHCHEGOLEVA N N, GABAY A M. Crystal structure of Zr_2Co_{11} hard magnetic compound [J]. Journal of Alloys and Compounds, 2007, 432: 135−141.

Zr−Co−Ge 三元体系在 1023、1173 和 1373 K 条件下的相平衡

胡 坤[1]，沈 忱[2]，刘华山[1]，张洪斌[2]

1. 中南大学 材料科学与工程学院，长沙 410083；

2. Institute of Materials Science, Technical University of Darmstadt, 64287 Darmstadt, Germany

摘 要：采用合金法并结合电子探针显微分析(EPMA)和 X 射线衍射(XRD)技术，精确测定 Zr−Co−Ge 三元体系在 1023、1173 和 1373 K 条件下的相平衡。合理构建 Zr−Co−Ge 体系在 1023、1173 和 1373 K 条件下的等温截面，分别包含 29、28 和 26 个三相区。除了证实文献中报道的 5 个三元化合物外，还检测到一个具有显著均匀性范围的新三元相 τ，其组成在 1023 K 时为 13.8%~19.4% Co (摩尔分数)，在 1173 K 时为 12.9%~19.0% Co (摩尔分数)和在 1373 K 时为 12.3%~14.9% Co (摩尔分数)。而且，推断一个零变量反应发生在 1023~1173 K，即 $\tau+\tau 1 \rightleftharpoons \tau 4+ZrGe_2$。此外，第三种元素 Ge 在一些 Co−Zr 中间相中可以部分替代 Co，如 $CoZr_2$ 和 $Co_{23}Zr_6$，其中，Ge 的最大溶解度分别可达 22.8% 和 20.3% (摩尔分数)。

关键词：Zr−Co−Ge 三元体系；相图；化合物；溶解度

(Edited by Wei-ping CHEN)